Date of publication xxxx 00, 0000, date of current version xxxx 00, 0000.

Digital Object Identifier 10.1109/ACCESS.2024.0429000

Flexible PCB Windings Size Optimization For Winding AC Resistance Minimization Under The Sinusoidal Voltage Regime

RAFAL P. WOJDA, (Senior Member, IEEE)
Oak Ridge National Laboratory, Energy Science and Technology Directorate, Electrification and Energy Infrastructure Division, Grid Systems Hardware Group, Knoxville, TN 37932, USA

Corresponding author: Rafal P. Wojda (wojdarp@ornl.gov)

Notice: This manuscript has been authored by UT-Battelle, LLC, under contract DE-AC05-00OR22725 with the US Department of Energy (DOE). The US government retains and the publisher, by accepting the article for publication, acknowledges that the US government retains a nonexclusive, paid-up, irrevocable, worldwide license to publish or reproduce the published form of this manuscript, or allow others to do so, for US government purposes. DOE will provide public access to these results of federally sponsored research in accordance with the DOE Public Access Plan (https://www.energy.gov/doe-public-access-plan).

ABSTRACT In this paper, optimization of the winding AC resistance of the flexible printed circuit board (FPCB) wire windings is performed. A one-dimensional model of the FPCB winding is introduced and an equation for the FPCB winding AC resistance and its low and medium frequency approximation are derived. The approximate FPCB winding AC resistance equation is used to derive optimum thickness of the FPCB winding conductor thickness at which minimum of winding AC resistance (global optimum) is achieved. The Finite Element Method analysis and experimental verification of derived equations (winding resistance, impedance, power loss, and temperature measurements) is performed in order validate derived model and winding resistance equation.

INDEX TERMS Eddy currents, Flexible Printed Circuit Board, Inductors and Transformers, Magnetic components, Winding optimization, Winding resistance, Winding loss.

I. NOMENCLATURE

γ - mass density of the material;
δ_w - skin depth of the winding conductor;
η - winding porosity factor;
κ - thermal conductivity of the material;
μ_0 - free space permeability;
μ_r - relative permeability of the core material;
μ_w - winding conductor permeability;
ρ_w - resistivity of the winding conductor;
ϕ - impedance phase shift;
ω - angular frequency;
b_f - foil width;
b_p - width of the FPCB wire path;
d - solid-round-wire winding diameter;
d_{str} - litz-wire winding strand diameter;
f - operating frequency;
f_r - resonant frequency;
f_s - switching frequency;
f_B - boundary frequency;
k_f - number of paths in the FPCB wire conductor;
k_{str} - number of strands in the litz wire bundle;
h_f - foil wire thicknesses;
h_p - FPCB wire path thickness;
l_e - mean magnetic path length (MPL);
l_w - winding conductor length;
l_T - mean turn length (MTL);
p - distance between center of conductors;
r - equivalent series resistance;
r_{calc} - calculated equivalent series resistance;
r_{meas} - measured equivalent series resistance;
x - equivalent series reactance;
A - effective thickness of the foil conductor winding;
A_f - effective thickness FPCB wire conductor winding;
A_{Cu} - cross-sectional area of the copper conductor;
A_{eff} - effective core cross-sectional area;
F_P - proximity effect factor;
F_R - winding AC-to-DC resistance ratio of the foil winding;
F_{Rflex} - winding AC-to-DC resistance ratio of the FPCB winding;
F_S - skin effect factor;
I_L - dc component of the current;
I_m - amplitude of the periodic current;

N - number of winding turns;
N_l - number of winding layers;
N_{ll} - effective number of winding layers;
N_{lp} - number of FPCB conductor layers;
RTI - relative thermal index;
R_w - winding AC resistance ;
R_{wdc} - winding DC resistance;
R_{wflex} - winding AC resistance of the FPCB winding;
$R_{wdcflex}$ - winding DC resistance of the FPCB winding;
T_{avg} - measured average temperature of the winding;
P_C - power loss of the core magnetic material;
V_e - volume of the core ;
Z - inductor impedance.

II. INTRODUCTION

HIGH efficiency and high quality factor inductive components (inductors and transformers) play a crucial role in modern power electronics. With considerably increasing switching frequencies of power converters and inverters, and motors, high-frequency high-performance magnetic components are of primary importance [1] - [30], especially those based on SiC and GaN modules. The high-frequency winding power loss of the litz-wire windings is taking significant part in the power system total efficiency. This is because for large current high-frequency applications, typically used copper litz-wire standard (0.1 mm and 0.071 mm diameter) suffers from a relatively high winding AC resistance, due to eddy current effects; skin and proximity effects. This fact has a significant impact on the quality factor of the inductor and its filtering capabilities as well as well as on winding loss.

The utilization of FPCBs as winding conductors in low-profile magnetic components—such as transformers and inductors—offers multiple advantages for high-frequency power conversion applications. Owing to their high winding window filling factor and extremely thin conductor paths, FPCB windings significantly reduce AC resistance at high frequencies, thereby improving efficiency. Compared to conventional planar PCB windings, which are typically constrained to conductor widths of approximately 100 µm due to fabrication limits, FPCBs can achieve path thicknesses an order of magnitude smaller. This reduction in thickness mitigates eddy current losses, enabling higher switching frequencies in DC-DC resonant converters. As a result, FPCB windings are particularly well-suited for both high-frequency power conversion and RF applications, where low-loss performance is critical. Furthermore, in medium-voltage (MV) converter designs, the superior window utilization of FPCBs allows a significantly higher number of turns to be accommodated within the magnetic core compared to traditional round wire windings. This increased turn density enhances the voltage handling and power delivery capabilities of the magnetic component, making FPCBs a viable solution for compact, high-performance magnetic integration across a wide range of applications.

In this paper, the Dowell's equation for the estimation of the winding AC resistance of the magnetic components like, inductor or transformer with magnetic core and FPCB windings [1] is used. The objectives of this paper are:

- To introduce the model of the FPCB windings,
- To adapt the one-dimensional winding model of the FPCB winding to the Dowell's equation for the winding AC resistance estimation,
- To approximate Dowell's equation for FPCB windings at low and medium frequencies,
- To derive equation for the optimum FPCB path thickness at which the minimum of the winding AC resistance is achieved,
- To compare the winding AC resistances of the solid-round-wire, litz-wire, and FPCB windings using Finite Element Method simulations with analytical derivation at high-frequencies,
- To compare the measured winding AC resistances of the solid-round-wire, litz-wire, and FPCB windings with analytical derivations.

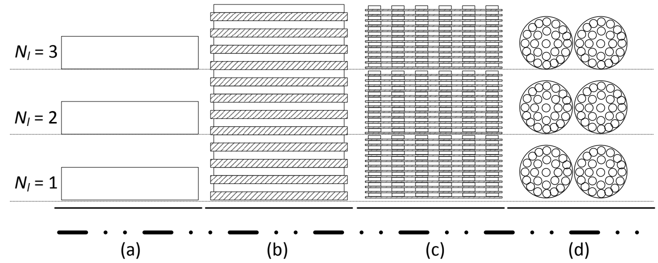

FIGURE 1. Structres of three layer $N_l = 3$ inductor with different winding conductors. (a) Foil winding inductor. (b) Thin foil winding inductor. (c) Flex-wire winding inductor. (d) Litz-wire winding inductor.

III. WINDING CONDUCTOR TYPES

Fig. 1 presents a three-layer inductor structures made of thick foil, thin foil, FPCB, and litz-wire conductors. Windings presented in this figure have unique properties, which allows them to be utilized in power applications at different frequency ranges. These properties will be shortly described in the following subsections.

A. THICK-FOIL WINDINGS

The thick-foil windings depicted in Fig. 1(a) are usually made of a wide and thick foil conductor whose thickness is greater than $h_f > 0.3$ mm. This type of winding is mainly used in the low-frequency high powers inductors and transformers. This is because at low frequencies the skin depth is relatively high and therefore, eddy currents induced in the winding conductor are negligible. As a result the winding resistance is considered equal to DC resistance of the current carrying conductor and the winding loss is considered equal to the DC loss.

Utilization of thick foil winding for high-frequency power applications cause that the skin depth of the current carrying conductor decreases (inversely proportional to the square root of frequency). As a result the eddy currents are not negligible

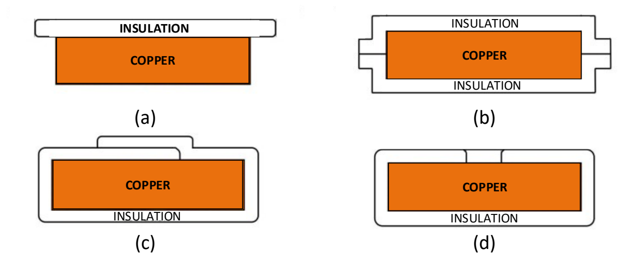

FIGURE 2. Insulated thin foil types [34]. (a) Type I. (b) Type II. (c) Type III. (d) Type IV.

anymore, and the winding AC resistance increases due to skin and proximity effects and so does the winding power loss.

The price of such windings is relatively low. This is because the manufacture process of the conductor is simple and the foil thickness is obtained by press rolling of the conductor sheets (cold or hot rolling). Winding layers of the foil inductor are usually separated with insulation sheets of thickness $t_{ins} \geq 0.1$ mm and typical materials used for insulation are; Nomex, Mylar, and Kraft or Fish Paper.

B. THIN-FOIL WINDINGS

The thin-foil windings illustrated in Fig. 1(b) are made with a foil conductor of thickness 35 μm$\leq h_f \leq 300$ μm, where the conductor laminations are attached to the insulation (glued or glueless). Thin foil laminations allow for utilization of such conductor in the high-frequency applications. This is because at high frequencies, induction of the eddy currents are restricted only by the conductor thickness. Thus, for the conductor made of thin copper foil with $h_f = 300$ μm the maximum operating frequency above which the eddy currents are induced is $f \approx 200$ kHz and for $h_f = 35$ μm the maximum operating frequency above which the eddy currents are induced is $f \approx 3.6$ MHz. The maximum operating frequency of the thin-foil conductor decreases as the conductor is used as a winding. This is because the proximity effect in the coil rapidly increases as the number of winding conductor layers increase.

Commonly, thin foils are parallelized in order to increase the current and the power capability of the magnetic component. In such cases, conductor terminals are electrically shunted on both ends of the conductor, while each thin foil is insulated with insulating material from adjacent foil along the whole length. Such conductor bundle is wound around the magnetic core. For example, thin copper foil winding can be made of Type 2 conductors (Fig. 2) [34], where the copper foil is insulated on both sides.

Table I lists the technical data and properties of the thin foils used as a winding conductor [34]. The variety of the insulating materials allows to utilize them in multiple applications depending on electrical, thermal, and flammability requirements [34]. Typical materials used for insulation material are; PET, Nomex®, and Kapton®, due to their high dielectric strength. The price of such a conductor can be 10 times (and more) higher than the regular thick foil conductor, and it depends on the insulation material and the way the conductor is insulated (Fig. 2).

Table I: Thin Foil Parameters

General	Copper	PET	Adhesive PET	Nomex®	Kapton®
Thickness (μm)	35-300	30	23	50	25
Thermal Class		B	B	F	H
Dielectric strength (kV)		6.4	4.5	2.0	6.0

C. SOLID-ROUND-WIRE WINDINGS

The solid-round-wire windings are commonly used in low-power high-frequency or high-power, low-frequency applications. This is because, in general, the cross-sectional area of the conductor depends only on the wire diameter and, therefore, for low-power high-frequency components, induction of eddy-currents is reduced by diameter reduction. For high-power, low-frequency components, the skin depth is relatively high, so the current flows through the whole conductor cross-sectional area; thus, the eddy currents are not induced.

Moreover, it has to be noted that the current and power capability of solid-round-wire windings depend on the insulation thermal class of the wire. This means that for a given insulation thermal class, the maximum current flowing through the conductor over the prolonged time, cannot cause any serious insulation degradation at any location along the wire length due to overheating. By increasing the conductor's cross-sectional area, it is possible to reduce the maximum thermal stresses subjected to the insulation by the current flow.

The price of the copper solid-round-wire is proportional to the copper price. This holds from 0000AWG up to $\approx$ 16AWG wire gauge. For higher gauges, the cost of the wire increases exponentially due to the fact that manufacture of a very thin strands requires multiple vacuum annealing of the copper during the drawing process.

D. LITZ-WIRE WINDINGS

Litz-wire is a bundle made of multiple insulated strands of equal diameter that are braided in order to assure higher flexibility (in comparison to the large diameter solid-round wire) during the winding of the bundle but also to prevent formation of the circulating eddy currents [3], [4], [8], [9], [10], [12], [14], [15], [16], [17], [18].

The litz-wire windings [35], [36], [41] [42] are typical solutions for the high-power high-frequency converter/inverter inductors and transformers.

This is because the wire consists of multiple thin wires that are braided or woven in order to utilization of very thin strands preclude induction of the eddy currents and increase of strand number in the litz-wire bundle allows for a larger total current to be conducted.

The winding AC resistance vs. frequency characteristics are shifted to higher frequencies in comparison to the foil windings and thus are suitable for the high-frequency power inductor and transformer design [3], [4]. Typically, litz wires are made of copper conductors. However, there are solutions made of aluminum and Copper-clad aluminum conductors [35], [36].

The price of the copper-litz wire windings depend on the complexity of braiding, insulation and on the strand diameter and strand number. In general, litz-wire windings price can be similar to the solid-round-wire windings but as complexity increase so does the price.

E. FLEXIBLE-PRINTED-CIRCUIT-BOARD WINDINGS

The FPCB conductor windings (Figs. 1, 3, and 8) are proposed for medium- and high-frequency inductor and transformer applications. The FPCB comprises polyimide (PI) base material and rolled and annealed copper conductor. The rolled annealed copper has good dynamic bending properties as well as very high purity ($\approx$ 99.9 %), yielding the low resistivity of copper $\rho_w \approx 17.24$ Ωnm. Such conductor has an excellent winding AC resistance vs. frequency properties mainly due to the fact that the induction of the eddy currents from the perpendicular magnetic field intensity is significantly reduced by the conductor path thickness (minimum path thickness is $h_{p(min)} \approx 8$ μm). Paths are electrically shunted at the beginning and end of the FPCB to ensure an even current distribution in each path. For relatively long FPCB conductors with thick paths, symmetrization of the current in each path can be achieved by variation of the path width at the terminal section in order to reduce the circulating eddy-currents [5]. Comparing to the thick and thin foil windings, the parasitic capacitance of the FPCB windings is much lower due to the fact that the copper surface between the turns is reduced. In [31], it has been shown that FPCB windings tend to have much lower losses than the standard FR4 PCB winding, and the steady-state temperature is 20 degrees Celsius lower for FPCB than that of the equivalent conventional FR4 PCB.

The flexible polymer substrate and wire layout of the thin FPCB makes it not the best candidate to operate with high currents. The higher current carrying requirements require thicker copper, especially when the design does not allow the utilization of wider traces. The thicker copper requires a thicker layer of adhesive in order to achieve a proper encapsulation (approximately 89 μm thick copper requires approximately 25 μm thick adhesive). The increase of the copper thickness causes the high-frequency ac resistance and loss to increase, and thus the main benefit of the FPCB to be used as a high-frequency winding conductor is defeated. However, the parallel connection of multiple FPCB's with thin copper paths, enables the conduction of relatively high currents. Additionally, implementation of the FPCB windings in the high-voltage applications is not a concern as the polyimide substrate breakdown voltage is approximately 6 kV per 25 μm of the PI film. The minimum bending radius requirements of the FPCB is specified by ANSI/IPC 2223, and it depends on the maximum allowable copper elongation, copper, insulation, and adhesive thicknesses. The rule of thumb for minimum radius bend requirements [39] for the single-layer FPCB is six times the FPCB thickness. Utilizing adhesiveless FPCB, where the copper is cast directly onto the polyimide core without the need of any adhesive, it is possible to reduce the thickness of the FPCB and thus reduce the minimum bend radius. The density of the PI film is approximately $\gamma_{PI} = 1420$ kg/m^3 and the density of copper is $\gamma_{Cu} = 8960$ kg/m^3 and the density of the FPCB is [32] $\gamma_{PI} = 3839$ kg/m^3. The thermal conductivity of the FPCB is $\kappa = 0.3$ W/(mK) [32]. Moreover, utilization of polyimide substrate allows for high temperature operation (up to 220 degree Celcius). The best application of the FPCB is for low profile components. The price of the FPCB windings is significantly higher than the price of the windings aforementioned, i.e., foils, solid-round and litz-wire windings. It depends on multiple factors like the number of layers in the FPCB conductor, thickness of the path, insulation thickness, complexity, length, type of encapsulation, and many others.

F. MECHANICAL PARAMETERS OF WINDING CONDUCTORS

Table II compares mechanical parameters of the foil, thin foil, solid-round-wire, litz-wire, and FPCB windings. RTI, γ, κ, are included for selected windings. It have to be notice that the thermal conductivity of the copper is κ_{Cu} = 398 W/(m·K) however, the copper windings thermal conductivity is significantly lower. In [33] and [32] steady-state measurements of thermal conductivity have been conducted for the litz-wire and FPCB conductors and results have been summarized in the Table II. In general, the winding thermal conductivity will depend on the many factors like surface area, insulation type, conductor distribution, ambient temperature, and therefore, the thermal conductivity will vary. Due to the fact that FPCB and thin foil conductors have relatively low thickness it is fairly easy to wind them around the core or bobbin as well as to keep high core winding window utilization factor. Conversely, large diameter litz- or solid-round-wire conductors require additional forces and winding a magnetic component maintaining high core winding window utilization factor may be sometimes very difficult. It is also worth of notice that thin foil and FPCB conductors can be rewound, while other wires like foil, solid-round and litz-wire are less likely to be rewound, due to physical deformation or insulation wear (except of served and extruded insulation).

IV. MODEL OF THE FPCB-WIRE WINDINGS

Fig. 3(a) shows a model of the multi-layer FPCB conductor. The FPCB conductor consists of k_f paths that are etched on the flexible polyamide substrate. The width of the path b_p as well as the distance between paths are technologically

Table II: Copper Windings Mechanical Parameters

Parameter	Foil	Thin Foil	Round	Litz	FPCB
RTI	$\geq$ H	H	H	H	H
Density γ (kg/m^3)	8960	$\leq$ 8960	$\approx$ 8960	$\leq$8960	3839
Thermal Conductivity κ (W/(m·K))				0.97 - 2.2	0.3 - 0.6
Min. Thickness/Diameter (μm)	$\geq$300	$\leq$300	25	25	8
Flexibility	Moderate	Good	Moderate	Moderate	Good
Rewinding	Low	Good	Low	Moderate	Good
Window Utilization	Moderate	Good	Moderate	Low	Good

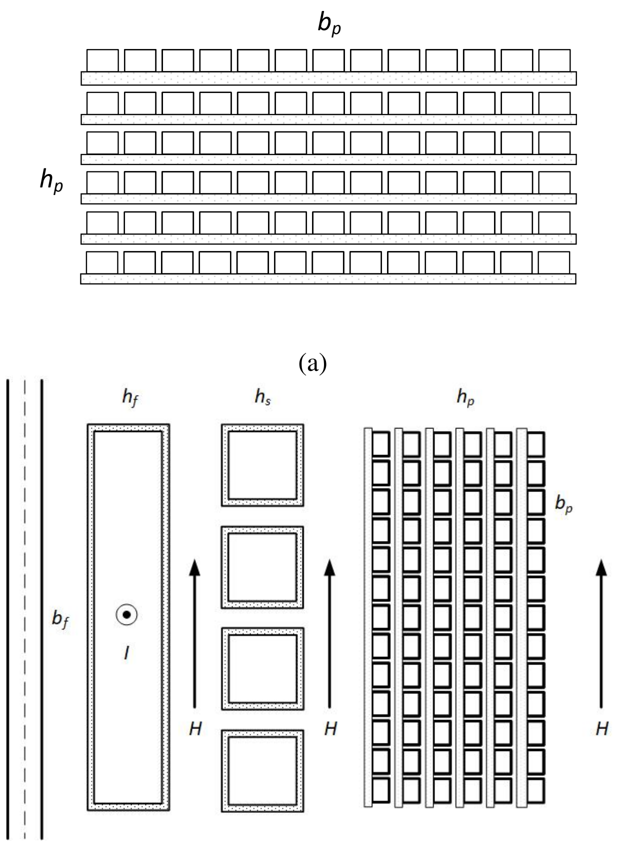

FIGURE 3. Model of FPCB conductor and its transformation. (a) Model of FPCB conductor. (b) Foil conductor to the FPCB conductor transformation.

restricted to ≈ 100 μm and cannot be reduced due to etching process. The minimum thickness of the path is $\approx$ 8 μm, however, further thickness reduction development is made in order to reduce it to 1 μm and less [34], [37], and [38].

The DC winding resistance of the FPCB wire is given by

$$R_{wdcflex} = \frac{\rho_w l_w}{b_p h_p k_f N_{lp}} = \frac{\rho_w l_T N}{b_p h_p k_f N_{lp}}. \tag{1}$$

Fig. 3(b) shows transformation of the foil winding to the FPCB winding. The winding AC resistance of the thick foil conductor was derived by Dowell [2] in 1966 directly form Maxwell's equations and is given by

$$F_R = \frac{R_w}{R_{wdc}} = A\left[F_S + \frac{2(N_l^2-1)}{3}F_P\right] \tag{2}$$

$$= A\left[\frac{\sinh(2A)+\sin(2A)}{\cosh(2A)-\cos(2A)} + \frac{2(N_l^2-1)}{3}\frac{\sinh(A)-\sin(A)}{\cosh(A)+\cos(A)}\right],$$

where $A = h_f/\delta_w$ is the effective thickness of the foil conductor and the skin depth of the conductor is given by

$$\delta_w = \sqrt{\frac{\rho_w}{\pi f \mu_0 \mu_w}}. \tag{3}$$

To adapt Dowell's equation to obtain the analytical expression of the FPCB winding AC resistance, the transition of the foil winding to the FPCB winding can be performed. By adjustment of the conductor resistivity, as well as the introduction of the porosity factor, i.e., the layer fill factor, one can convert the foil conductor into several equivalent conductors to ensure that the DC winding resistance remains unchanged. A transformation of the foil winding (Fig. 3(b)) requires replacement of the wide foil sheet with several narrow rectangular conductors [3]. Then the rectangular conductors are replaced with narrower and thinner paths.

The DC winding resistances of the foil conductor is given by

$$R_{wdc} = \frac{\rho_w l_w}{b_f h_f} = \frac{\rho_w l_T N_l}{b_f h_f}. \tag{4}$$

Equating (1) and (4) one obtains the required number of paths for the FPCB winding

$$k_f = \frac{b_f h_f}{b_p h_p N_{lp}}. \tag{5}$$

For the FPCB winding conductor as shown in Fig. 3(b),

$$A_f = \frac{h_p}{\delta_w}\sqrt{\frac{b_p}{p}} = \frac{h_p}{\delta_w}\sqrt{\eta}. \tag{6}$$

The total number of layers in the FPCB winding depends of the FPCB conductor layers N_{lp} and is given by

$$N_{ll} = N_l N_{lp}. \tag{7}$$

As the current and power capability of the inductor increases, the number of layers in the conductor also should increase.

For the single-layer FPCB conductor ($N_{lp} = 1$), the AC-to-DC winding resistance ratio is given by

$$F_{Rflex} = \frac{R_{wflex}}{R_{wdcflex}} = A_f \left[\frac{\sinh(2A_f) + \sin(2A_f)}{\cosh(2A_f) - \cos(2A_f)} + \frac{2(N_l^2 - 1)}{3} \frac{\sinh(A_f) - \sin(A_f)}{\cosh(A_f) + \cos(A_f)} \right]. \quad (8)$$

For the multi-layer FPCB conductor ($N_{lp} > 1$), the AC-to-DC winding resistance ratio is given by

$$F_{Rflex} = \frac{R_{wflex}}{R_{wdcflex}} = A_f \left[\frac{\sinh(2A_f) + \sin(2A_f)}{\cosh(2A_f) - \cos(2A_f)} + \frac{2(N_l^2 N_{lp}^2 - 1)}{3} \frac{\sinh(A_f) - \sin(A_f)}{\cosh(A_f) + \cos(A_f)} \right] = A_f \left[\frac{\sinh(2A_f) + \sin(2A_f)}{\cosh(2A_f) - \cos(2A_f)} + \frac{2(N_{ll}^2 - 1)}{3} \frac{\sinh(A_f) - \sin(A_f)}{\cosh(A_f) + \cos(A_f)} \right], \quad (9)$$

where N_{ll} is the effective number of winding layers with the multi-layer FPCB conductor. The winding AC resistance of the FPCB winding is given then by

$$R_{wflex} = \frac{\rho_w A_f l_w}{b_p h_p k N_{lp}} \left[\frac{\sinh(2A_f) + \sin(2A_f)}{\cosh(2A_f) - \cos(2A_f)} + \frac{2(N_l^2 N_{lp}^2 - 1)}{3} \frac{\sinh(A_f) - \sin(A_f)}{\cosh(A_f) + \cos(A_f)} \right]. \quad (10)$$

Fig. 4 shows the winding AC resistance of the FPCB conductor as a function of the path thickness.

V. OPTIMIZATION OF THE FLEXIBLE PRINTED CIRCUIT BOARD WINDINGS

Design of the FPCB windings usually requires defining the required path thickness and the number of paths in the conductor. To derive the optimum path thickness, the number of winding layers and the number of conductor layers must be constant. By extending skin and proximity effect factors of the equation (9) into Maclaurin's series and substituting them into that equation, the approximation of the FPCB winding resistance ratio is achieved

$$F_{Rflex} = \frac{R_{wflex}}{R_{wdcflex}} - 1 + \frac{5N_l^2 N_{lp}^2 - 1}{45} A_f^4, \quad \text{for } A_f \leq 2. \quad (11)$$

The approximate winding AC resistance is given by

$$R_{wflex} = \frac{\rho_w l_w}{b_p k_f N_{lp}} \left(\frac{1}{h_p} + \frac{5N_l^2 N_{lp}^2 - 1}{45\delta_w^4} h_p^3 \right), \quad \text{for } A_f \leq 2. \quad (12)$$

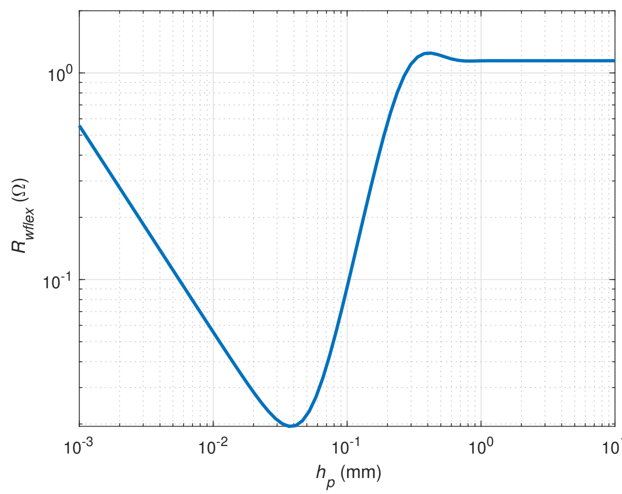

FIGURE 4. The winding AC resistance of the FPCB winding for the conductor with $k = 155$, $b_p = 100$ μm $N_{lp} = 2$, and $N = 10$ at $f = 260000$ Hz.

By taking derivative of (12) with respect to path thickness and equating it to zero

$$\frac{dR_{wflex}}{dh_p} \approx \frac{\rho_w l_w}{b_p N_{lp} k} \left[\frac{1}{h} + \frac{3\eta^2 (5N_l^2 N_{lp}^2 - 1) h_p^2}{45\delta_w^4} \right] = 0, \quad (13)$$

one obtains the normalized path valley thickness at which the winding AC resistance has minimum value

$$\frac{h_{pv}}{\delta_w} = \sqrt[4]{\frac{15}{(5N_l^2 N_{lp}^2 - 1)\eta^2}}. \quad (14)$$

The AC-to-DC winding resistance ratio at the normalized path valley thickness is

$$F_{Rflexv} = 1 + \frac{\eta^2 (5N_l^2 N_{lp}^2 - 1)}{45} \left(\sqrt[4]{\frac{15}{(5N_l^2 N_{lp}^2 - 1)\eta^2}} \right)^4 = \frac{4}{3}. \quad (15)$$

From (15) and from behavior of the FPCB winding AC resistance shown in Fig. 4 it can be seen as the FPCB windings behave like foil windings instead of like, litz wire winding, and thus increasing the number of paths does not increase the winding AC resistance at high frequencies.

VI. FEM ANALYSIS

In this section, FEM simulations of the FPCB, litz, and solid-round-wire windings are performed. The Ansys Maxwell 2D simulation environment was used to build and simulate three inductors with different types of windings, as shown in Fig. 5. The eddy current solver was selected to predict winding resistances over the wide frequency range. The relatively small sizes of the wire and core were selected to reduce the computational time with approximately 1,200,000 mesh elements for the FPCB winding, 400,000 mesh elements for the litz-wire winding, and 180,000 mesh elements for the solid-round-wire winding. The aim of the FEM simulations was to investigate the behaviour of the winding resistances at

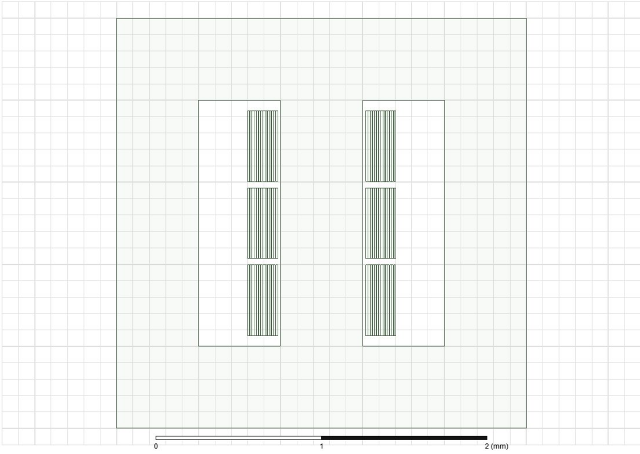

(a)

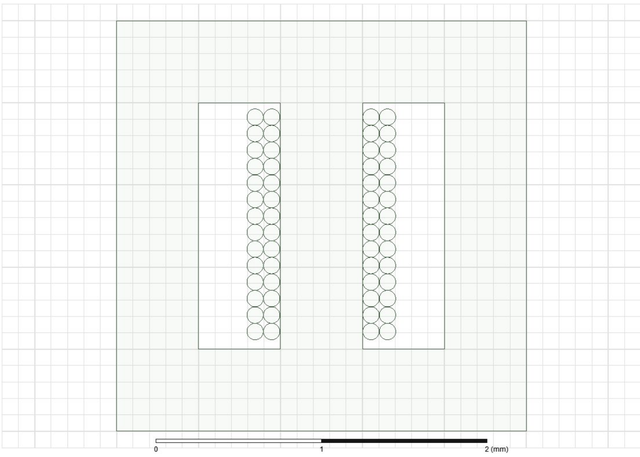

(b)

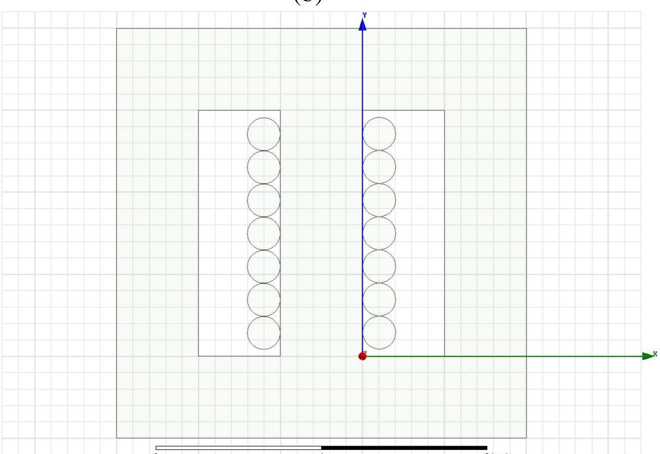

(c)

FIGURE 5. **2D FEM model of simulated inductors. (a) Model of FPCB winding inductor. (b) Model of litz-wire winding inductor. (c) Model of solid-round-wire winding inductor.**

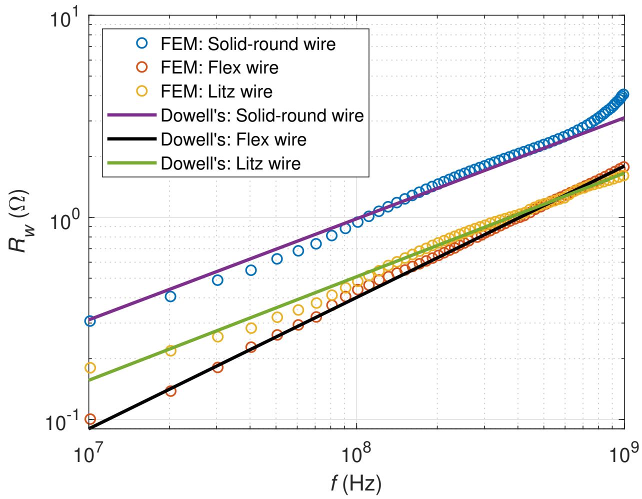

FIGURE 6. **FEM simulated and Dowell's estimations of winding AC resistance for FPCB, litz-wire, and solid-round-wire winding inductors.**

high frequencies and to validate the derived equations (9) and (10). The dimensions of the analyzed wire windings were:

- FPCB-wire, with $k_f = 3$, $h_p = 24$ μm, and $b_p = 436$ μm
- Litz-wire, with $k_{str} = 4$, and $d_{str} = 100$ μm,
- Solid-round-wire, with $d = 140$ μm.

For all of these windings, the copper cross-sectional area was $A_{Cu} \approx 0.31416$ mm^2, thus the DC resistance was similar for all wires and it was approximately equal $R_{wdc} \approx 15.4$ mΩ.

Moreover, the ferromagnetic EE gap-less core was selected for the FEM simulations, and it was the same for all windings. For further reduction of the computational time and effort the relative magnetic permeability of the core material was independent of frequency (constant permeability vs. frequency), and it was a linear function of magnetic field intensity as well as the air insulation was used for all of winding conductors. Using the AC current source with the current amplitude of $I_m = 1$ A FPCB-, litz-, and solid-round-wire windings winding AC resistances were calculated.

Fig. 6 compares the winding AC resistance for FPCB-wire, litz-wire, and solid-round-wire winding inductors calulated using FEM simulations and Dowell's equations. It can be seen that Dowell's equation very well captures FEM simulated winding resistance for the solid-round-wire and the litz-wire windings. The first winding AC resistance increase is for the solid-round-wire winding, the second is for the litz-wire winding, and the third is for FPCB-wire winding.

For the solid-round-wire windings, the Dowell's equation precisely predicts the FEM simulated winding resistance up to 10 MHz, where the resistance of the wire is 20 times higher than the DC resistance. As the frequency increases the Dowell's equation overestimates the winding resistance maximum by 13% at 50 MHz, and underestimates the winding resistance maximum by 30% at 1 GHz. For the litz-wire windings, the Dowell's equation underestimates the winding AC resistance by 1 % at 10 MHz and then in the frequency range 20-150 MHz overestimate the simulated resistance maximally by 2.8 %. For the FPCB-wire windings, the Dowell's equation underestimates the winding AC resistance maximally by 3% for frequencies 10-100 MHz, and for frequencies larger than

Table III: Winding Conductor Parameters

General	Round	Litz	FPCB
Diameter/Thickness (μm)	644	202	21
Path Width (μm)	-	-	100
No of paths/strands	-	10	155
Conductor layers	1	$\sqrt{k} \approx 3$	$N_{lp} = 1$

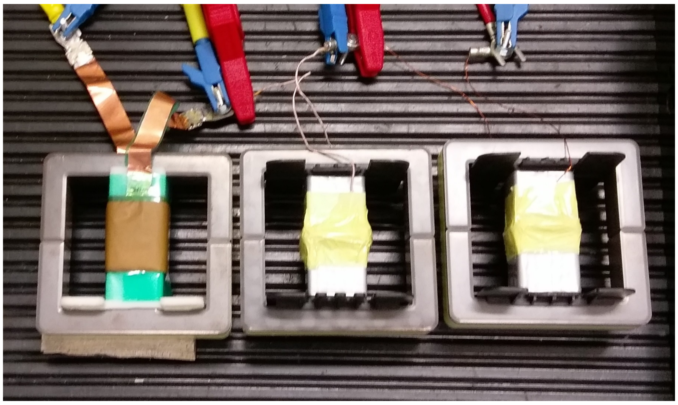

FIGURE 7. Photo of measured three inductors wound with FPCB (left), litz-wire (center), and solid-round-wire (right) windings.

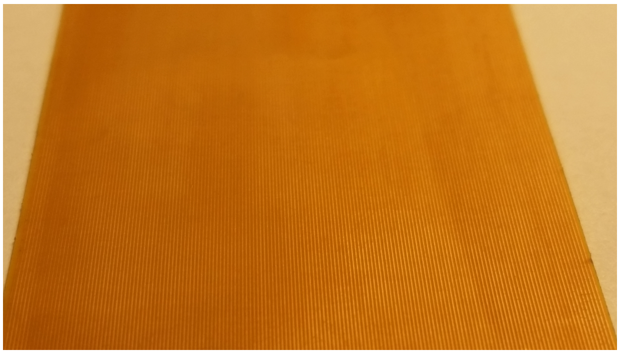

FIGURE 8. Photo of the FPCB conductor [38].

100 MHz the Dowell's equation tracks the FEM simulated resistance with high accuracy.

Moreover, it can be seen that the FPCB-wire has lower than the litz-wire winding AC resistance in the 10 -30 MHz range, then in the 30MHz$< f <$ 70MHz the resistance is higher and in the 70MHz$< f <$ 450MHz resistance is lower than that of the litz-wire winding. Above 500 MHz, the winding AC resistance of the FPCB winding is higher than that of the litz-wire winding due to the proximity effect caused by large number of effective winding layers.

VII. MEASUREMENTS

In this section, experimental verification of the FPCB-wire winding AC resistance (10) is done. Impedance and loss comparison for three powder core inductors were made. Fig. 7 shows a photo of the built inductors and winding parameters are listed in Table III.

The core of the measured inductors was EE-shape Mega-Flux core EK8038A060μ, with powder relative permeability $\mu_r = 60$ [40]. This core has: $l_e = 18.5$ cm, $A_{eff} = 3.89$ cm^2,

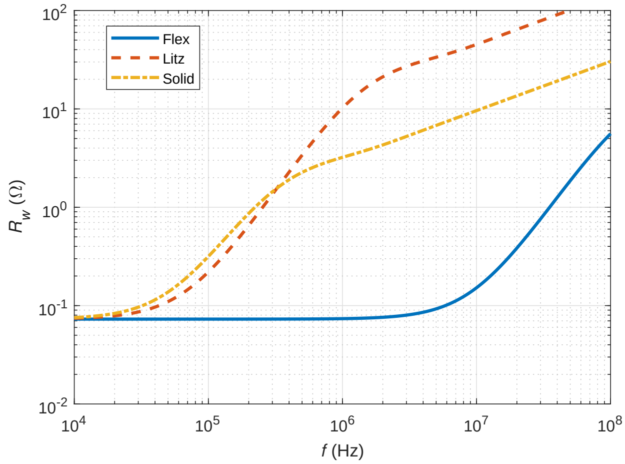

FIGURE 9. Calculated winding AC resistances for FPCB-wire (solid), litz-wire (dashed), and solid-round-wire (dash-dot) winding inductors.

and inductance factor $A_L = 190$ nH/N^2. Each inductor consisted of $N = 9.5$ turns and the inductance of inductors was $L \approx 17$ μH. The inductors were wound with the following winding conductors:

- Solid-round-wire winding 22AWG ($\approx$ 0.6243 mm wire diameter) with $A_{Cu} = 0.3257$ mm^2,
- Litz-wire winding 10 x 32AWG ($\approx$ 0.2032 mm strand diameter) with $A_{Cu} = 0.3205$ mm^2,
- and single layer FPCB-wire conductor with $h_p = 21$ μm, $b_p \approx 100$ μm, and $A_{Cu} = 0.3255$ mm^2 and $k_f = 155$ (Fig. 8).

The FPCB winding had polyimide (PI) film thickness of t_{ins} =12.5 μm. The length of the conductor was $l_w = 900$ mm and the parallel paths were spaced by 100 μm, yielding $\eta = 0.5$. The width of the tape was 31 mm.

Fig. 9 shows the calculated winding AC resistances using (10) of the solid-round-wire, litz-wire, and FPCB-wire windings. Note that the low-frequency region of the winding AC resistance for the FPCB-wire windings is the widest from the analyzed windings. The boundary frequency f_B, (it is a frequency at, which the ac resistance is higher than the DC winding resistance by 5% [21]) for the measured FPCB-wire winding was approximately $f_B \approx 2$ MHz. Moreover, it can be seen that the solid-round wire has the narrowest low-frequency region and the boundary frequency was approximately $f_B \approx 8$ kHz, whereas the boundary frequency of the litz-wire winding was approximately $f_B \approx 20$ kHz. Additionally, it can be seen that as frequency increases to approximately 300 kHz, the litz-wire winding AC resistance is lower than that of the solid-round-wire winding, however, above 300 kHz litz-wire winding AC resistance is significantly higher than that of the solid-round-wire winding.

A. IMPEDANCE MEASUREMENTS

It is impossible to measure directly the winding resistance R_w at frequencies close to the self-resonant frequency because

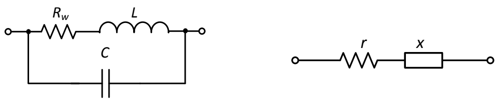

(a) (b)

FIGURE 10. Equivalent circuit of inductors with negligible core losses. (a) Lumped-parameter equivalent circuit. (b) Equivalent series circuit.

of the inductor self-capacitance [3], [4], [19]- [21], and [24]. A lumped-parameter model of the inductor, neglecting the core losses, is depicted in Fig. 10. The model of the inductor consists of self-inductance L, winding AC resistance R_w, and parasitic self-capacitance C [3] and [4]. Additionally, the model may contain core resistance R_c in series with winding AC resistance R_w. However, in the subsequent analysis, the core resistance is neglected. This is because, using 4294A Precision Impedance Analyzer, the core loss is very low at low values of the magnetic flux density $B \approx 93$ μT. Therefore, neglecting the core resistance [3] and [4], the impedance of the equivalent circuit depicted in Fig. 10 is

$$Z = \frac{R_w}{(1-\omega^2 LC)^2 + (\omega C R_w)^2} \qquad (16)$$

$$+ j\omega L \frac{1-\omega^2 LC + (CR_w^2/L)}{(1-\omega^2 LC)^2 + (\omega C R_w)^2} = r + jx = |Z| e^{j\phi}.$$

Fig. 11 shows the measured impedance magnitude $|Z|$ and the phase ϕ as functions of frequency for the solid-round- , litz-, and FPCB-wire winding inductors. It can be seen that the impedance magnitude $|Z|$ for the FPCB-wire winding inductor is the lowest up to frequency $\approx$ 2 MHz. Moreover, it can be seen that the resonant frequencies for FPCB-wire winding inductor is the lowest among the measured inductors and it was $f_r = 4.375$ MHz. For the solid-round- and litz-wire windings, resonant frequency were $f_r = 15.1$ MHz, and $f_r = 15.7$ MHz, respectively. The reason for the low resonant frequency of the FPCB-wire winding inductor is relatively large surface area of the winding conductor yielding large self-capacitance of the inductor. It can be reduced by increasing insulation thickness or by adding spacers between the layers. The winding DC resistance was $R_{wdc} \approx 72.9$ mΩ for all windings. Table IV compares the measured and calculated winding resistances of the inductors. It can be seen that for $f = 260$ kHz, the calculated ESR is close to the measured one.

Characterization of the AC resistance in the vicinity of the self-resonant frequency is critical, particularly in applications involving high-frequency current conduction [25]-[27]. This is often the case in high-frequency (HF) power converters and radio-frequency (RF) power amplifiers [23], where the frequency spectrum content extends well beyond the fundamental switching frequency. Accurate estimation of resistance in this frequency range is essential not only for predicting overall efficiency but also for reliably assessing the thermal performance of magnetic components.

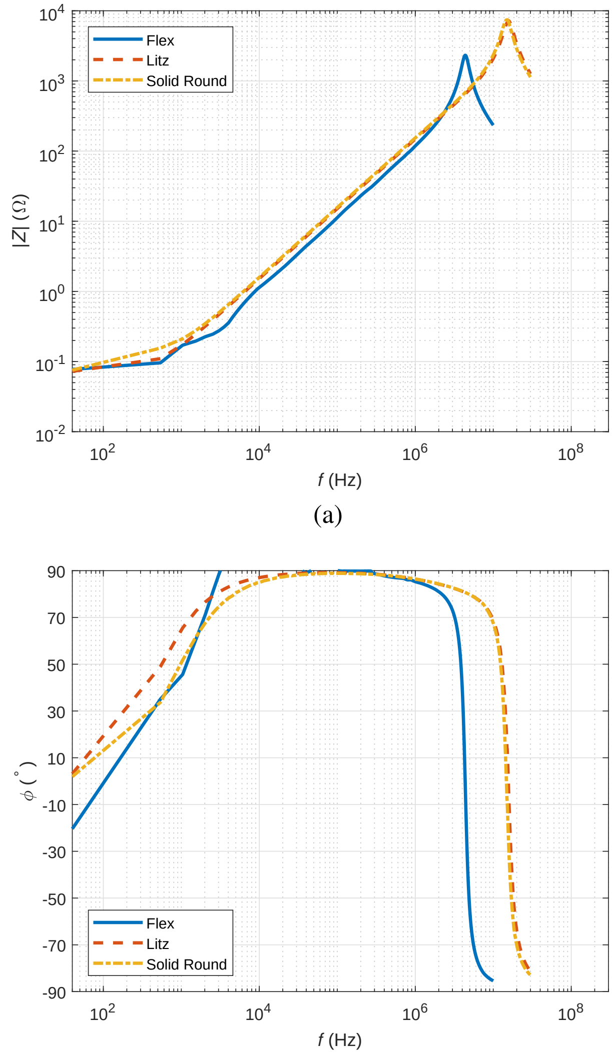

(b)

FIGURE 11. Plots of measured impedance Z as function of frequency for the solid-round- (dash-doted line), litz- (dash line), and FPCB-wire (solid line) winding inductors. (a) Measured |Z| as function of frequency. (b) Measured ϕ as function of frequency.

Although harmonic components are typically lower in amplitude than the fundamental, their contribution to power loss and thermal stress can be significant. Furthermore, at very high frequencies, the magnetic permeability of core materials may decrease due to intrinsic material limitations. This degradation in permeability alters the effective impedance, leading to increased harmonic currents and elevated high-frequency winding losses.

B. POWER LOSS MEASUREMENTS

Fig. 12 shows winding power loss measurement setup. It consists of SiC H bridge inverter made of 4 $\times$ CREE C3M0065090 N-Channel Planar MOSFET. The inverter was supplied from the DC voltage source. The switches were

Table IV: Comparison of measured and calculated inductor series resistances at $f = 260$ kHz

Winding Type	$\lvert Z\rvert e^{j\phi}$ (Ω)	r_{meas} (Ω)	r_{calc} (Ω)	R_w (Ω)
FPCB	$29.6e^{j89.85}$	0.07599	0.07348	0.073
Litz	$39.56e^{j88.53}$	1.0149	1.0424	1.0418
Solid	$40.98e^{j88.32}$	1.2014	1.2179	1.2172

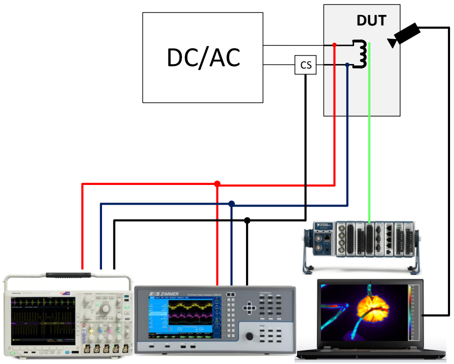

FIGURE 12. **Inductor winding power loss measurement setup.**

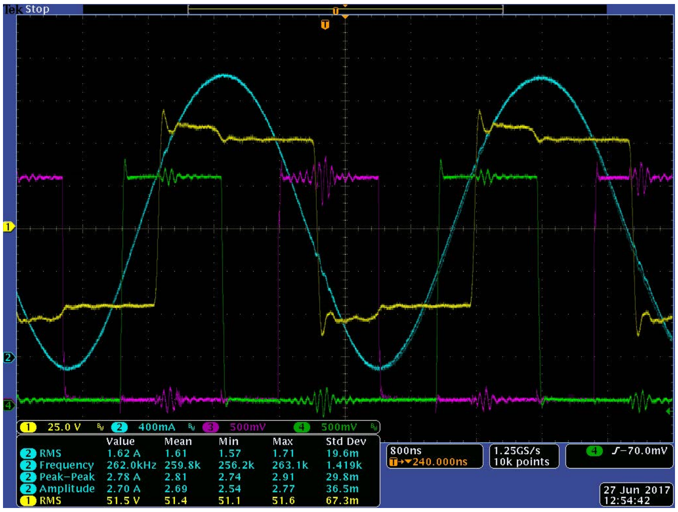

FIGURE 13. **Measured waveforms (CH1 (Yellow) Inductor voltage waveform , CH2 (Cyan) inductor current , CH3 (Purple) and CH4 (Green) gate driver voltage waveforms .**

controlled with STM32FR programmable generator. The inductor voltage and current waveforms were observed using Tektronix A622 current probe and Tektronix MSO 4054B oscilloscope. The power losses of the inductor were measured using ZES Zimmer LMG670 power analyzer.

The frequency of the inductor current was $f_s \approx 260$ kHz, the DC current was $I_L = 1.2$ A, the RMS current $I_{RMS} = 1.3948$ A, and the amplitude of the fundamental component was $I_m = 1.72$ A, as shown in Fig. 13.

Additionally, inductor temperature measurements were performed in order to investigate the influence of the core temperature rise on the winding loss as well. Inductor temperatures were acquired using Flir IR thermal camera and and

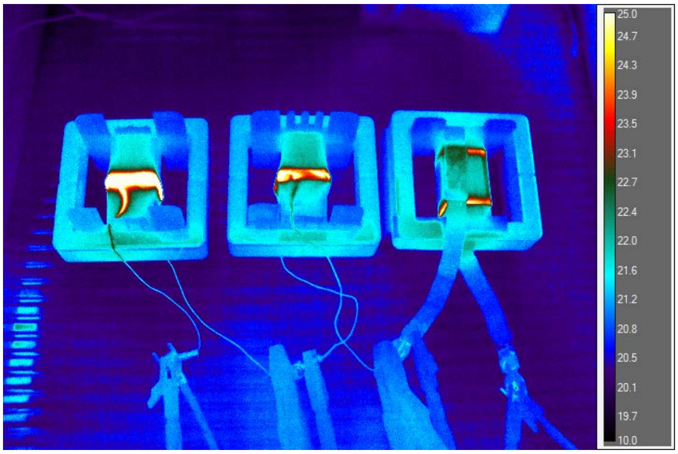

FIGURE 14. **Thermal images of measured inductors Solid-round-wire winding inductor (left), Litz-wire winding inductor (center), and FPCB-wire winding right).**

NI CompactDAQ data acquisition system.

No significant influence of the core temperature on the winding loss was identified. This is because the core temperature was kept at the same temperature level as before tests were performed, i.e., $T_c = 21.6$ °C as shown in Fig. 14. The average winding temperatures were

- Solid-round-wire winding inductor $T_{avg} = 27.8$ °C,
- Litz-wire winding inductor $T_{avg} = 24.2$ °C,
- FPCB-wire winding $T_{avg} = 22.1$ °C.

The calculated magnetic flux density was

$$B = \frac{\mu_0 \mu_r N I_m}{l_e} \approx 8 \text{ (mT)}. \tag{17}$$

For the calculated magnetic field density, the core loss was

$$P_C = \frac{(10B)^{2.145}(8.874 f_{kHz} + 0.0632 f_{kHz}^{1.980})V_e}{1000} = 1.9475 \text{ (W)}. \tag{18}$$

The calculated winding loss are given in Table V. Figs. 15 shows the measured waveforms of the power loss for the litz-wire, FPCB, and solid-round-wire winding inductors. Table V compares the calculated and measured inductor power loss (for the winding current shown in Fig. 13) and list the relative error between the measured and calculated loss values. It can be seen that the lowest power loss was for the FPCB-wire winding inductor. Additionally, errors ϵ between the measured and calculated values were listed for each winding types. Calculations of the power loss for the FPCB winding were underestimated by 11.44 % and overestimated by 2.73 % and 1.67 % for the litz-wire and solid-round-wire windings, respectively.

It has to be noted that the main assumption of one-dimensional (1-D) winding model and equations derived in this paper is similar to the one that was derived by Dowell. Dowell's assumed straight parallel foil conductors, yielding parallel magnetic field to the foil conducting layers. Due to transformation performed in Section IV, magnetic field is not parallel to the conducting layers and magnetic field exhibit

Table V: Power Loss Comparison at $f = 260$ kHz

Winding Type	Measured Loss (W)	Calculated Winding Loss (W)	Calculated Total Loss (W)	Relative Error (%)
FPCB	2.478	0.2469	2.1945	-11.44
Litz	3.971	2.1317	4.0792	2.73
Solid	4.348	2.4729	4.4205	1.67

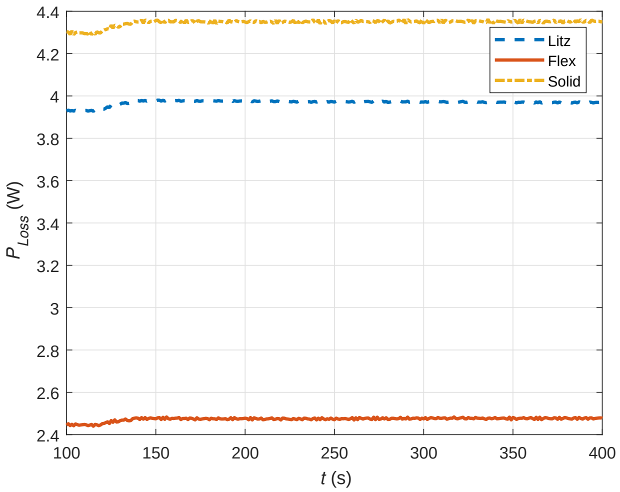

FIGURE 15. Waveforms of the measured power loss as function of time for litz-wire, FPCB and solid-round-wire winding inductors.

circumferential and perpendicular components along with the parallel component and thus for modeling of these magnetic field components 2-D analysis is required. For modeling a longitudinal magnetic field component the 3-D analysis is required. Therefore, there will be difference in results when comparing 1-D, 2-D, 3-D analysis, and measurements as it is shown above in this Sections VI and VII.

VIII. CONCLUSION

The one-dimensional model of the FPCB-wire winding has been introduced and equation for the calculation of the FPCB winding AC resistance has been derived. The closed-form winding AC resistance equation has been approximated, and optimization of the FPCB path thickness to achieve the minimum winding AC resistance (global minimum) has been derived. The derived model was verified with the FEM simulations. It has been shown that at very high frequencies, the 1-D model and 2-D model exhibit mismatch in resistance estimation and with the maximum error 13% at $\approx$ 50 MHz and $\approx$ 1 GHz.

The experimental verification of derived equations has been performed and impedance and power loss measurements have been performed. From the impedance measurements, it has been shown that the calculated ESR and measured ESR of the FPCB-wire winding, were captured with high accuracy. Additionally, it has been shown that the FPCB winding inductors have relatively low self-resonant frequency (comparing to litz and solid) due to large conductor surface area yielding the large parasitic self-capacitance. Moreover, it has been shown that the winding AC resistance of the FPCB was lower than the solid-round-wire and the litz-wire windings at medium and high-frequency range of the winding AC resistance.

From the power loss measurements, it has been showed that the FPCB windings loss was the lowest. For the operating frequency $f_s = 260$ kHz, the measured power loss was, $\approx 2.4,\ 3.9,\ 4.4$ W for the FPCB, litz-wire and solid-round-wire windings, respectively. The derived model for the FPCB winding AC resistance tracked the equivalent series resistance of the FPCB-wire winding inductor with high accuracy however, the calculated power loss was underestimated approximately by 11 %. The thermal measurements showed that the temperature of the FPCB winding was the lowest comparing to equivalent (with the same winding DC resistance) solid-round-wire winding and litz-wire winding inductor.

Comparison of the solid-round wire, litz-wire and FPCB-wire windings showed, that the winding AC resistance of the FPCB was lower than the solid-round-wire and the litz-wire windings at medium and high-frequency range of the winding AC resistance. The power loss measurements showed that the FPCB windings loss was the lowest. For the operating frequency $f_s = 260$ kHz, the measured power loss was, $\approx 2.4,\ 3.9,\ 4.4$ W for the FPCB, litz-wire and solid-round-wire windings, respectively. Moreover, the measured temperature of the tested winding inductors was the lowest for the FPCB-wire winding inductor.

REFERENCES

[1] R. P. Wojda, “Resistance of The Flex-Wire Windings," *2022 IEEE Energy Conversion Congress and Exposition (ECCE)*, October 2022.
[2] P. L. Dowell, “Effects of eddy currents in transformer winding," *Proc. IEE*, vol. 113, no. 8, pp. 1387-1394, Aug. 1966.
[3] M. K. Kazimierczuk, *High-Frequency Magnetic Components.* John Wiley & Sons, Chichester, UK, 2013.
[4] R. P. Wojda and M. K. Kazimierczuk, “Winding resistance of litz-wire and multi-strand inductors," *IET, Power Electron.*, vol. 5, no. 2, pp. 257-268, Feb. 2012.
[5] R. P. Wojda, A. Polit, M. Wawro, and G. Molinski “High-frequency winding from PCB printed circuits," PL422409A1, 02.11.2019.
[6] E. Bennett and S. C. Larsen, “Effective resistance of alternating currents of multilayer windings," *Trans. Amer. Inst. Elect. Eng.*, vol. 59, pp. 1010-1017, 1940.
[7] M. P. Perry, “Multiple layer series connected winding design for minimum losses,"*IEEE Transactions on Power Apparatus and Systems*, vol. PAS-98, no. 1, pp. 116-123, January/February 1979.
[8] P. N. Murgatroyd, “Calculation of proximity losses in multistranded conductor branches," *IEE Proceedings,* Part A, vol. 136, no. 3, pp. 115-120, May 1989.
[9] J. A. Ferreira, “Analytical computation of AC resistance of round and rectangular litz-wire windings," *IEE Proceedings, Part B, Electric Power Applications,* vol. 139, no 1, pp. 21-25, Jan. 1992.
[10] J. A. Ferreira, “Improved analytical modelling of conductive losses in magnetic components," *IEEE Trans. Power Electron.,* vol. 9, no. 1, pp. 127-131, Jan. 1994.
[11] M. Bartoli, N. Noferi, A. Reatti, and M. K. Kazimierczuk, “Modeling winding losses in high-frequency power inductors," *Journal of Circuits, Systems and Computers,* vol. 5, no. 4, pp. 607-626, Dec. 1995.
[12] M. Bartoli, N. Noferi, A. Reatti, and M. K. Kazimierczuk, “Modeling litz-wire winding losses in high- frequencies power inductors," Proceedings of the IEEE Power Electronics Specialists Conference, Baveno, Italy, June 24-27, 1996. pp. 1960-1966.

[13] M. Bartoli, A. Reatti, and M. K. Kazimierczuk, “Minimum copper and core losses power inductors design," Proceedings of the 1996 Thirty-First IEEE Industry Applications Society IAS Annual Meeting, Oct. 1996, pp. 1369-1376.
[14] A. W. Lotfi, F. C. Lee, “A high frequency model for litz wire for switch-mode magnetics," Proc. of the 1993 IEEE Industry Applications Society Annual Meeting, vol. 2, 1993, pp. 1169-1175.
[15] J. Acero, P. Hernandez, J. M. Burdio, R. Alonso, and L. A. Barragan, “Simple resistance calculation in litz-wire planar windings for induction cooking appliances," *IEEE Transactions on Magnetics,* vol. 41, no. 4, pp. 1280-1288, April 2005.
[16] J. Schutz, J. Roudet, and A. Schellmanns, “Modeling litz-wire windings," Proc. IEEE Industry Appl. Soc. Annual Meeting (IAS), New Orleans, LA, October 5-9, 1997, vol. 2, pp. 1190-1195.
[17] G. W. O. Howe, “The high-frequency resistance of multiply-stranded insulated wire," *Proc. Royal Soc. Lon.* A, vol. 93, pp. 468-492, September 1917.
[18] T. Guillod, J. Huber, F. Krismer, and J. W. Kolar, “Litz Wire Losses:Effects of twisting Imperfections," 2017 IEEE 18th Workshop on Control and Modeling for Power Electronics (COMPEL), Stanford, CA, USA, July 9 - 12, 2017.
[19] R. P. Wojda and M. K. Kazimierczuk,“Analytical optimization of solid-round wire windings," *IEEE Trans. Ind. Electron.*, vol. 60, no. 3, pp. 1033-1041, 2013.
[20] R. P. Wojda, “Thermal analytical winding size optimization for different conductor shapes," *The Journal of Polish Academy of Sciences, Archives of Electrical Engineering*, vol. 64, no. 2, pp. 197-214, 2015.
[21] R. P. Wojda and M. K. Kazimierczuk , “Analytical optimisation of solid-round-wire windings conducting dc and ac non-sinusoidal periodic currents," *IET, Power Electron.*, vol. 6, no. 7, pp. 1462 – 1474, 2013.
[22] R. P. Wojda and M. K. Kazimierczuk , “Analytical winding size optimisation for different conductor shapes using Ampère’s Law," *IET, Power Electron.*, vol. 6, no. 6, pp. 1058 – 1068, 2013.
[23] R. P. Wojda and M. K. Kazimierczuk , “Maximum drain efficiency class F3 RF power amplifier," IEEE International Symposium of Circuits and Systems, Rio de Janeiro, Brazil, May 15-18, 2011.
[24] R. P. Wojda and M. K. Kazimierczuk , “Analytical optimization of litz-wire windings independent of porosity factor," *COMPEL: The Int. Journal for Computation and Mathematics in Electrical and Electronic Engineering,* vol. 34, no. 3, pp. 920-940, 2015.
[25] R. P. Wojda and M. K. Kazimierczuk , “Analytical optimisation of solid-round-wire windings conducting dc and ac non-sinusoidal periodic currents," *IET, Power Electron.*, vol. 6, no. 7, pp. 1462 – 1474, 2013.
[26] R. P. Wojda and M. K. Kazimierczuk , “Analytical winding foil thickness optimisation of inductors conducting harmonic currents," *IET, Power Electron.*, vol. 6, no. 5, pp. 963 – 973, 2013.
[27] R. P. Wojda and M. K. Kazimierczuk , “Optimum foil thickness of inductors conducting DC and non-sinusoidal periodic currents," *IET, Power Electron.*, vol. 5, no. 6, pp. 801 – 812, 2012.
[28] P. Han, D. Lawhorn, Y. Chulaee, D. Lewis, G. Heins, D. M. Ionel, “Design Optimization and Experimental Study of Coreless Axial-flux PM Machines with Wave Winding PCB Stators," 2021 IEEE Energy Conversion Congress and Exposition (ECCE), Vancouver, BC, Canada, Oct. 10-14 2021, doi:10.1109/ECCE47101.2021.9595963.
[29] F. Baudart, B. Dehez, J. Denies, M. Markovic and Y. Perriard, “Shape optimization of flexible PCB slotless windings in BLDC machines," 2013 International Conference on Electrical Machines and Systems (ICEMS), Busan, Korea (South), 2013, pp. 943-948, doi: 10.1109/ICEMS.2013.6754395.
[30] C. Clonts,“The push for e-propulsion progress," *SAE Automotive Engineering,* vol. 10, no.2, pp. 16 - 20, March 2023.
[31] M. Ngo, Y. Cao, D. Dong, R. Burgos, J. Noon, and H. Kouns, “Design and Comparison of FR4 and Flex PCB Transformer for High Frequency High Current Low Profile Applications," 2023 IEEE Applied Power Electronics Conference and Exposition, Orlando, FL, USA Mar. 19-23, 2023.
[32] I. Ahmad, M.S. Abdul Aziz, M.Z. Abdullah, M. A. A. M. Salleh, M. H. H. Ishak, W. Rahiman, and M. Nabialek“Investigations of Infrared Desktop Reflow Oven with FPCB Substrate during Reflow Soldering Process," *Open Access Metallurgy Journal*, DOI:10.3390/met11081155, July 2021.
[33] X. Liu, D. Gerada, and Z. Xu, “Effective Thermal Conductivity Calculation and Measurement of Litz Wire based on the Porous Metal Materials Structure," *IEEE Transactions on Ind. Electronics,* vol. 67, no. 4, pp. 2667-2677, April 2019.
[34] http://www.synflex.com
[35] http://hflitzwire.com
[36] https://www.elektrisola.com/home.html
[37] http://ats.net/
[38] www.qflexinc.com
[39] https://www.epectec.com/
[40] www.changsung.com
[41] http://www.elettrofili.it
[42] https://bulkwire.com

ACKNOWLEDGMENT

The author gratefully acknowledges Marcin Pietrzycki, formerly with the ABB Corporate Research Center in Krakow, Poland, for his contributions to the development of the high-frequency testing setup.

RAFAL P. WOJDA (Senior Member, IEEE) received B.S. and M.S. degrees (summa cum laude) in electronics engineering from the Institute of Radioelectronics and Multimedia Technology at Warsaw University of Technology, Poland, in 2007 and 2009, respectively. He completed his Ph.D. in electronics at Wright State University, Dayton, OH, USA, in 2012, with a focus on microwave engineering, VLSI, and nanotechnology. During 2009–2010, he was awarded a Fulbright Scholarship to conduct research at Wright State University.

From 2012 to 2018, Dr. Wojda was a Senior Scientist at the ABB Corporate Research Center in Krakow, Poland, where he led the development and optimization of magnetic components for power conversion systems. His work advanced technologies in renewable energy, electric vehicle charging, power protection, and transportation electrification.

Since 2018, he has been a Research and Development Staff Member at Oak Ridge National Laboratory (ORNL). His research focuses on high-frequency and medium-voltage magnetic components, with emphasis on loss modeling, thermal management, and insulation design. He also contributes to the development of advanced magnetic technologies for solid-state transformers, wireless power transfer systems, and energy-efficient hardware for exascale computing platforms.

Dr. Wojda has authored numerous peer-reviewed publications and has received several distinctions, including the IET Power Electronics Premium Award for Best Paper in 2014. He is an alumnus of both the Fulbright Program and the U.S. Department of State Exchange Program.

He is actively involved in the professional community as Chair of the IEEE East Tennessee PELS/PES Joint Chapter and serves as Secretary of the IEEE Power Electronics Society Technical Committee on Design Methodologies (TC10).